Journal of Inflammation Research

Dovepress
Taylor & Francis Group

Open Access Full Text Article

ORIGINAL RESEARCH

The Alterations in the Osteoimmune Microenvironment of STZ-Induced Type 2 Diabetic Mice:A Single-Cell RNA Sequencing Analysis

Ke Han[1], Shuang G Yan[2], Fanxiao Liu[1], Lianxin Li[1], Dongsheng Zhou[1], Lin Li[3], Nan Liu[1], Jinlei Dong[1]

[1]Department of Orthopaedics, Shandong Provincial Hospital Affiliated to Shandong First Medical University, Jinan, Shandong, People's Republic of China; [2]Department of Orthopaedic Surgery, The First Affiliated Hospital of Anhui Medical University, Hefei, Anhui, People's Republic of China; [3]Department of Orthopedic Surgery, Tengzhou Central People's Hospital Affiliated to Jining Medical University, Tengzhou, Shandong, People's Republic of China

Correspondence: Jinlei Dong, Department of Orthopaedics Shandong Provincial Hospital affiliated to Shandong First Medical University, Jinan, Shandong, People's Republic of China, Email dongjinlei@163.com

Background: This study aimed to delineate the single-cell transcriptome of bone marrow (BM) cells from wild-type (WT) and type 2 diabetic (T2D) mice, revealing distinct immune microenvironment features.

Methods: Single high-throughput single-cell RNA sequencing dataset (GSE212726) from BM cells of WT and streptozotocin (STZ)-induced T2DM mice were analyzed. Uniform manifold approximation and projection (UMAP), pseudo-time analysis, gene enrichment studies, and CellphoneDB were employed to identify immune cell interactions within the osteoimmune microenvironment. Key gene expression was validated by quantitative real-time polymerase chain reaction (qRT-PCR).

Results: After filtering low-quality cells and doublets, 9,360 cells (WT) and 10,885 cells (T2DM) were retained and classified into 12 clusters. Proportional analysis revealed a significant decrease in BM-neutrophils (66.56% → 54.73%) and an increase in B cells (9.16% → 19.78%) in the DM group. The DM/WT ratio for BM-neutrophils/T cells, BM-neutrophils/DCs, and monocytes/T cells increased, while the ratio for BM-neutrophils/Naïve_B decreased. KEGG pathway analysis highlighted enrichment of neurodegeneration, protein processing in the endoplasmic reticulum, and amyotrophic lateral sclerosis pathways in BM-neutrophils. Intercellular communication analysis indicated reduced incoming and outgoing interaction strength for B cells and T cells, while the T2D group showed enhanced THBS, VISFATIN, CLEC, IL4, and IL6 signaling. Notably, CLEC was specific to outgoing signaling in T cells, and THBS was specific to both outgoing and incoming signaling in monocytes, MSCs, and BM-neutrophils.

Conclusion: Single-cell RNA sequencing provides a comprehensive profile of bone marrow immune cells in T2D mice and has highlighted their heterogeneity, population shifts, and intercellular interactions. These findings highlight critical alterations in immune cell functions that may contribute to T2D progression and suggest possible avenues for future therapeutic investigation. Future research should continue to leverage scRNA-seq technology to refine treatment strategies and enhance patient outcomes by addressing immune dysfunction and chronic inflammation.

Keywords: single-cell RNA sequencing, bone marrow, diabetes mellitus, osteoimmunology, lymphocyte

Introduction

Type 2 diabetes mellitus (T2DM) is a chronic metabolic disorder marked by insulin resistance and relative insulin deficiency, leading to persistent hyperglycemia. Unlike Type 1 diabetes mellitus (T1DM), which typically arises in childhood and involves autoimmune destruction of pancreatic β-cells, T2DM predominantly occurs in adults and is strongly associated with obesity, physical inactivity, and genetic predisposition.[1,2] The rising global prevalence of T2DM underscores the urgent need to elucidate its pathophysiology, particularly the interplay between metabolic dysregulation, systemic inflammation, and tissue-specific complications, including those affecting the bone marrow.

Received: 17 June 2025
Accepted: 29 October 2025
Published: 4 November 2025

Chronic low-grade inflammation is increasingly recognized as a central contributor to T2DM progression. Immune cells, such as monocytes, macrophages, and neutrophils, mediate this inflammatory state, exacerbating insulin resistance and metabolic dysfunction. The bone marrow (BM), as the primary hematopoietic organ, serves both as a source and a regulator of these immune cells. Consequently, alterations in BM cellular composition and function can profoundly influence systemic inflammation, immune responses, and metabolic homeostasis.[3,4] Notably, T2DM has been associated with an expansion of pro-inflammatory monocytes (eg, Cd36+ subsets) and skewing of macrophage polarization towards a pro-inflammatory phenotype, suggesting that immune dysregulation in the BM may contribute to both chronic inflammation and impaired bone remodeling.[5,6] Furthermore, changes in the BM microenvironment, including stromal cell activity and extracellular matrix remodeling, can disturb hematopoiesis and immune responses, linking local BM alterations to systemic complications of T2DM such as cardiovascular disease and kidney injury.[7–9]

Bone health is tightly connected to BM immune regulation, a relationship encapsulated by the concept of osteoimmunology. Immune cells within the BM, including monocytes, neutrophils, and B cells, influence osteoclast and osteoblast activity, thereby modulating bone formation and resorption. In T2DM, chronic hyperglycemia, metabolic stress, and inflammatory cytokines disrupt the balance of osteoclasts and osteoblasts, increasing the risk of osteoporosis and fracture.[10–12] For instance, AP-1–mediated suppression of osteoclast activity has been described in diabetic bone, underscoring how molecular immune signals can reshape skeletal remodeling.[13] Importantly, emerging evidence indicates that immune-mediated shifts in BM neutrophils, B cells, and monocytes not only impair local bone turnover but also exacerbate systemic inflammation and metabolic dysfunction, further connecting osteoimmune interactions to broader T2DM pathophysiology. Clinically, such immune-driven bone fragility has been associated with higher fracture incidence, delayed bone healing, and poorer outcomes after orthopedic surgery in diabetic patients, making this research area of significant translational relevance. Despite these insights, detailed mechanisms linking specific BM immune subsets to T2DM-related bone pathology remain poorly understood. A deeper understanding of how immune dysregulation contributes to T2DM and its complications is crucial for the development of targeted prevention and treatment strategies of bone health.[14,15]

Technological advances such as single-cell RNA sequencing (scRNA-seq) now provide a transformative approach to dissect cellular heterogeneity and functional states at unprecedented resolution. This technology is particularly suited for studying the BM microenvironment in T2DM, where multiple immune and stromal cell types interact dynamically, and conventional bulk RNA-seq approaches cannot resolve subset-level changes or intercellular signaling networks.[16,17] Previous scRNA-seq studies[16,17] in diabetic models have explored general shifts in myeloid and lymphoid compartments; however, they often lack detailed subset annotation, functional state analysis, or ligand-receptor interaction characterization, leaving gaps in understanding BM immune dysregulation in T2DM.[18,19] Thus, the precise mechanisms linking BM immune alterations to systemic inflammation and bone pathology in T2DM remain incompletely understood.

To address these knowledge gaps, the present study leverages scRNA-seq to provide a comprehensive analysis of BM cells in T2DM mice. Specifically, our objectives are to: (1) profile immune cell heterogeneity, including neutrophil, monocyte, B cell, T cell, and dendritic cell subsets; (2) identify T2D-specific alterations in cellular proportions and functional states; and (3) characterize intercellular communication within the osteoimmune microenvironment through ligand-receptor analysis. By systematically mapping these changes, we highlight nuanced T2D-specific reprogramming of the BM immune landscape, uncover altered pathways such as THBS, CLEC, and IL-6 signaling, and provide mechanistic insights into how BM immune dysregulation contributes to systemic inflammation, insulin resistance, and bone remodeling defects in T2DM. Collectively, this study not only extends beyond prior research by integrating cellular, molecular, and intercellular dimensions of BM pathology, but also lays the foundation for future translation of scRNA-seq findings into therapeutic strategies that may alleviate immune dysfunction and skeletal complications in T2DM.

Materials and Methods

High-Throughput Gene Expression Data

The high-throughput single-cell RNA sequencing data were downloaded from the GEO database (https://www.ncbi.nlm.nih.gov/geo/) under the accession number GSE212726. The dataset is based on the GPL24247 platform (Illumina NovaSeq 6000, Mus musculus) and includes two samples: whole bone marrow cells extracted from the femur and

tibia of wild-type mice (Group WT) and those from T2DM mice (Group DM). These samples were selected for in-depth analysis in this study. This dataset was selected due to its comprehensive annotation, availability of metadata, and complete profiling of bone marrow immune cells. Other public datasets (eg, db/db or diet-induced models) were also screened through GEO and ArrayExpress using the terms: "diabetes", "bone marrow", "single-cell RNA-seq", "mouse", and "immune." Inclusion criteria required (a) availability of raw counts or processed matrices, (b) annotation of bone marrow tissue origin, (c) specification of diabetes induction method, and (d) sufficient sequencing depth and metadata. While GSE212726 was prioritized, future studies will incorporate additional murine and human datasets for validation and translational extension.

Cell Clustering Analysis, Visualization, and Annotation

To ensure data quality, Low-quality cells (<200 detected genes or >10% mitochondrial transcripts) and potential doublets (>25,000 UMIs) were excluded. Additional doublet detection was performed using DoubletFinder v2.0. Data normalization and regression were performed with Seurat v5.0.3, generating scaled data from UMI counts and mitochondrial content. For cell normalization and regression, we utilized the Seurat package (version 5.0.3, https://satijalab.org/seurat/). The process involved using the expression matrix, unique molecular identifier (UMI) counts per sample, and mitochondrial content to generate scaled data. Principal Component Analysis (PCA) was performed on the top 2,000 highly variable genes, and the first 10 principal components were selected for constructing t-SNE and UMAP plots. To address batch effects across samples, we applied the fastMNN function from the scran package (version 1.12.1) with parameters set to k=5, d=50, and approximate = TRUE, leveraging the mutual nearest neighbor method. An unsupervised cell clustering analysis was performed using a graph-based method with a resolution of 0.4, focusing on the top 10 PCA components. The identification of marker genes was conducted via the FindAllMarkers function, utilizing the Wilcoxon rank sum test algorithm with the following criteria: (1) log fold change (logFC) greater than 0.25; (2) p-value less than 0.05; (3) minimum percentage (min.pct) exceeding 0.1. To refine cell type characterization, clusters identified as the same cell type were selected for additional re-tSNE analysis, followed by graph-based clustering and marker identification.

Pseudo-Time Analysis

Pseudotime analysis was performed using Monocle 2 [Monocle2](http://cole−trapnell−lab.github.io/monocle−release), utilizing the DDR-Tree algorithm with default settings. Before running the Monocle analysis, we selected marker genes identified from the Seurat clustering results and utilized raw expression counts of filtered cells. Following the pseudotime analysis, Branch Expression Analysis Modeling (BEAM)[20] was employed to investigate genes responsible for determining cell fate at specific branch points.

Cell-Cell Communication Analysis

We used CellphoneDB v 2.1.7,[21] a comprehensive database of ligands, receptors, and their interactions, to systematically examine cell-cell communication molecules. For clusters at various time points, we annotated membrane, secreted, and peripheral proteins. We identified significant interactions by evaluating the mean interaction scores and cell communication significance, considering only those interactions with a p-value less than 0.05. These interactions were based on the normalized cell matrix obtained through Seurat's normalization process. Normalized Seurat matrices were input, and results highlight potential T2D-specific signaling (eg, THBS, CLEC, IL-6). These predictions are computational and require experimental confirmation (eg, blocking antibodies, co-culture assays).

Differential Expression Genes (DEGs) Analysis

To identify differentially expressed genes (DEGs) among samples, we utilized the FindMarkers function, which employs the Wilcoxon rank-sum test algorithm. The criteria for selecting DEGs were as follows: a logFC greater than 1, an adjusted p-value below 0.05, and a minimum expression percentage (min.pct) above 0.1.

Gene Ontology Analysis

To understand the biological significance of marker genes and DEGs, we conducted Gene Ontology (GO) analysis. GO annotations were sourced from NCBI (http://www.ncbi.nlm.nih.gov/), UniProt (http://www.uniprot.org/), and the Gene Ontology database (http://www.geneontology.org/). Fisher's exact test was applied to identify significantly enriched GO categories, and we adjusted p-values using False Discovery Rate (FDR) correction.[22]

Pathway Analysis

Pathway analysis was conducted to identify key pathways associated with marker genes and DEGs by leveraging the KEGG database.[23] Significant pathways were selected using Fisher's exact test, with p-values and FDR serving as thresholds for significance. Particular attention was given to osteoimmunology-relevant pathways.[24]

Quantitative Real-Time Reverse Transcription Polymerase Chain Reaction (qRT–PCR)

Type 2 diabetes mellitus (T2DM) was induced in C57BL/6J mice by feeding a high-fat diet (HFD, D12492, Research Diets; 60% kcal from fat) for 8 weeks, followed by a single low-dose intraperitoneal injection of streptozotocin (STZ, 100 mg/kg, Sigma). This HFD+STZ combination model is widely used to mimic the pathophysiology of T2DM, as HFD induces insulin resistance and low-dose STZ causes partial β-cell dysfunction. Successful induction of T2DM was confirmed by measuring fasting blood glucose levels (>11.1 mmol/L), impaired glucose tolerance tests (GTT), and increased body weight compared with WT controls. Control mice received a standard chow diet. Bone marrow samples from three mice per group, were harvested from the femur and tibia for s **qRT–PCR**. Although a formal power analysis was not conducted prior to sample collection due to the high cost and complexity of scRNA-seq, we acknowledge this as a limitation and note that future studies with larger cohorts will be needed to further validate these findings. We acknowledge that the small sample size limits statistical power, and STZ-induced diabetes may have cytotoxic effects independent of hyperglycemia; complementary models such as db/db or diet-induced T2D will be needed in future studies. For validation experiments, key genes, including FOSB, RELB, IL1B, MAP3K7, PPP3R1, TNF, TGFBR2, and SOCS3, were selected for qRT-PCR analysis using RNA extracted from the bone marrow of diabetic (DM) and control (WT) groups. Purified DNA-free RNA was isolated using the RNeasy Mini Kit, reverse transcribed using the One Step PrimeScript® miRNA cDNA Synthesis Kit (Takara, Japan, D350A), and amplified using the SYBR® Premix Ex Taq™ II Kit (Takara, Japan, DRR820A), following the manufacturer's instructions. Gene expression levels were calculated using the ΔΔCT method after normalization to the expression of the GAPDH housekeeping gene. Primer sequences used for qRT-PCR are provided in Supplementary Table 1. Each reaction was performed in triplicate technical replicates for each of the three biological samples per group. Melt curve analysis was conducted to confirm amplification specificity.

Statistical Analysis

All statistical analyses and data visualizations were conducted using R software (version 4.3.3). GraphPad Prism software (version 8.1.0; GraphPad Software Inc., USA) was used to perform statistical analyses and generate graphs.[25] One-way analysis of variance (ANOVA) was applied to compare gene expression levels and inflammatory factor concentrations. For comparisons between two groups, unpaired two-tailed Student's t-tests were used. For multiple group comparisons, one-way ANOVA followed by Tukey's post hoc test was applied. Proportional changes were assessed with chi-square tests. Results were presented as means ± standard errors (SEM), and a p-value of less than 0.05 was considered statistically significant.

Results

Profiles of Bone Marrow Cells in WT and T2D Mice

The high-throughput scRNA-seq data were downloaded under accession number GSE212726. In total, 10,420 cells from WT mice and 11,577 cells from T2D mice were collected. After filtering low-quality cells and duplicates, 9,360 cells from WT and 10,885 cells from T2D mice were retained for analysis (Figure 1A). Unbiased clustering identified 12 distinct cell populations: monocytes (primarily expressing Ass1, Trem2, and Lgals1), basophils (primarily expressing Prss34, Mcpt8, and Gata2), BM-

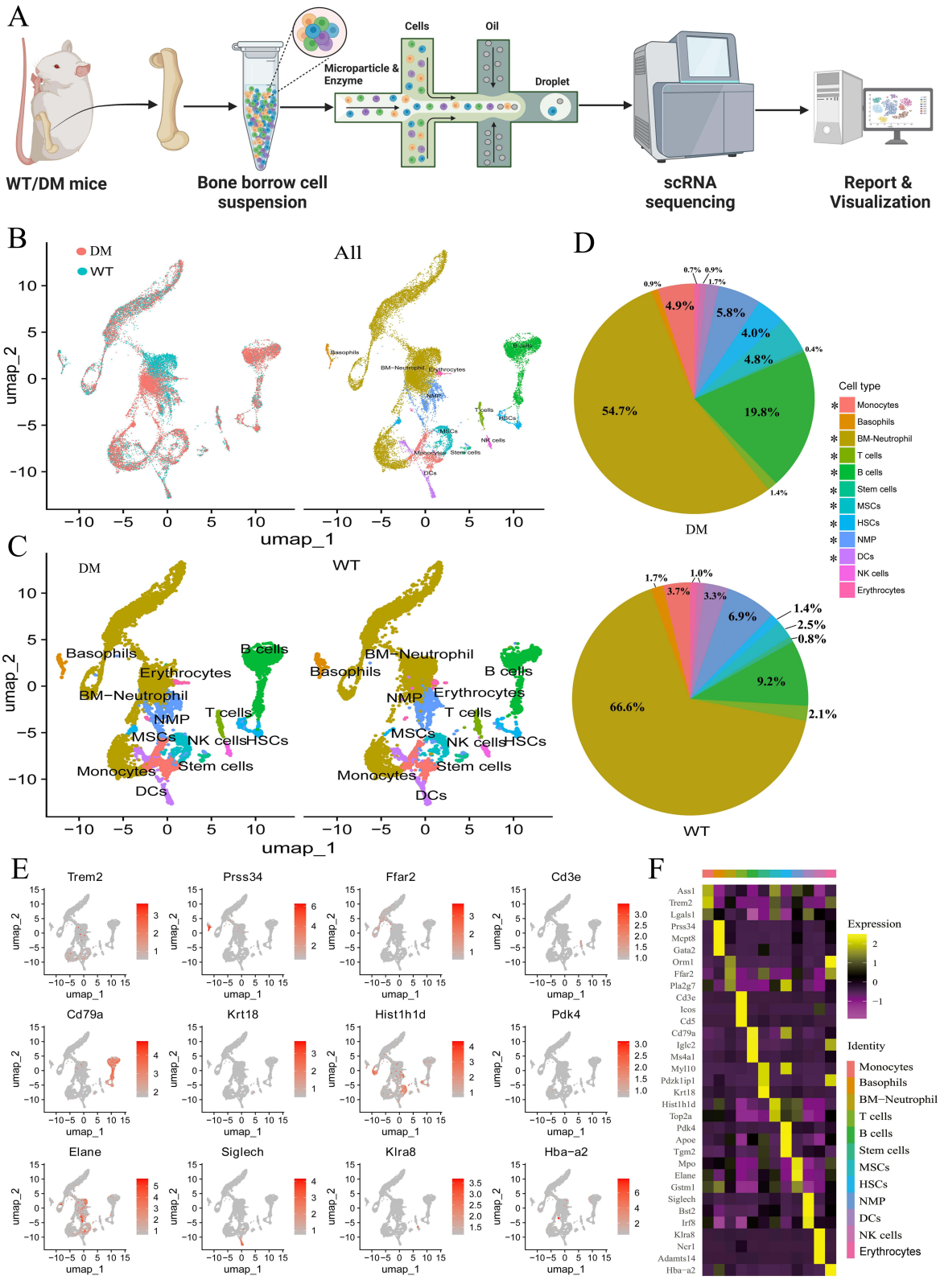

Figure 1 Single-cell RNA sequencing provide a comprehensive atlas of bone marrow cells in WT and T2D mice. (**A**) Study overview. (**B-C**) Clustering of bone marrow cells into twelve distinct clusters. (**B**) UMAP of unbiased clustering of all bone marrow cells in groups WT and DM; (**C**) UMAP of unbiased clustering and cell annotation of bone marrow cells in group WT and DM, respectively. (**D**) The proportions of each cell in groups WT and DM;*:p < 0.05. (**E**) Key cell type marker genes of 12 cell clusters, the redder the color, the higher the expression. (**F**) Cluster signature genes highlighted on left. Expression of top differentially expressed genes (rows) across the cells (columns), the warmer the color, the higher the expression.

https://doi.org/10.2147/JIR.S544316

neutrophils (primarily expressing Orm1, Ffar2, and Pla2g7), T lymphocytes (T cells, primarily expressing Cd3e, Icos, and Cd5), B lymphocytes (B cells, primarily expressing Cd79a, Iglc2, and Ms4a1), stem cells (primarily expressing Myl10, Pdzk1ip1, and Krt18), mesenchymal stem cells (MSCs, primarily expressing Hist1h1d and Top2a), hematopoietic stem cells (HSCs, primarily expressing Pdk4, Apoe, and Tgm2), neutrophil-myeloid progenitors (NMP, primarily expressing Mpo, Elane, and Gstm1), dendritic cells (DCs, primarily expressing Siglech, Bst2, and Irf8), NK cells (primarily expressing Klra8, Ncr1, and Adamts14), and erythrocytes (primarily expressing Hba-a2) (Figure 1B–F).

Cell proportion analysis revealed significant differences between WT and T2D mice. B cells (9.16% → 19.78%), MSCs (2.50% → 4.80%), monocytes (3.72% → 4.92%), and HSCs (1.36% → 4.00%) increased, while BM-neutrophils (66.56% → 54.73%), DCs (3.25% → 1.71%), basophils (1.68% → 0.89%), T cells (2.08% → 1.37%), and NMPs (6.94% → 5.82%) decreased. Stem cells, erythrocytes, and NK cells exhibited slight decreases. The top increases and decreases were observed in B cells and BM-neutrophils, respectively (Figure 1D).

Heterogeneity of BM-Neutrophils in the Bone Marrow of T2D Mice

M-neutrophils exhibited the largest proportional reduction. Six subsets were identified: BM-neutrophil_0 (primarily expressing Mpo, Elane, and Gstm1), BM-neutrophil_1 (primarily expressing Slfn5, Mpeg1, and Wfdc17), BM-neutrophil _2 (primarily expressing Retnlg, Ceacam10, and Mmp9), BM-neutrophil_3 (primarily expressing Orm1, Tmem216, and Zmpste24), BM-neutrophil_4 (primarily expressing Chit1, Fcnb, and Mogat2), and BM-neutrophil_5 (primarily expressing Clec4d, Vnn3, and Cstdc4) (Figure 2A–D).

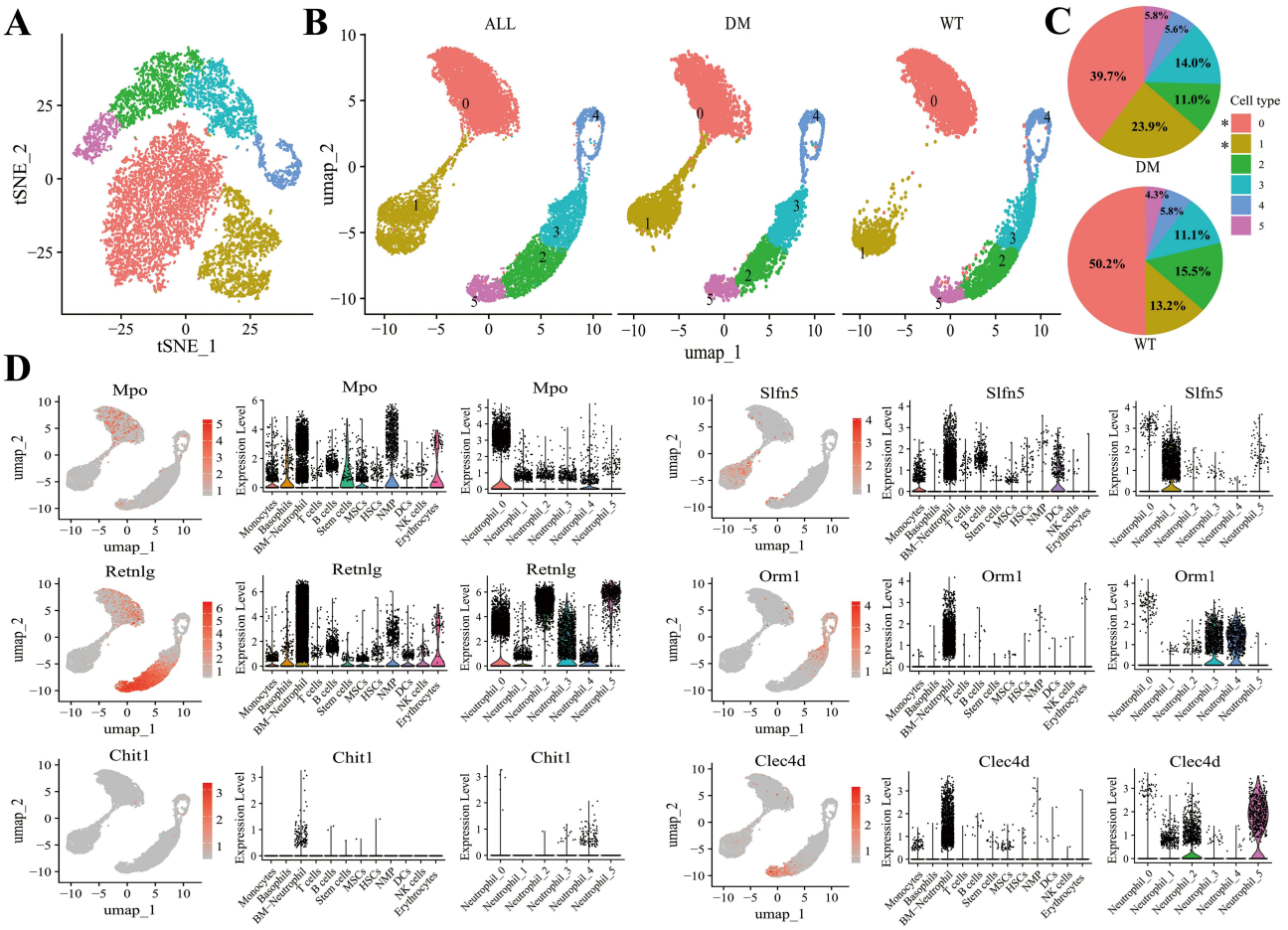

Figure 2 The characteristics of BM-neutrophils between groups WT and DM. (**A**) The tSNE results of BM-neutrophil cluster among all cells. (**B**) UMAP of BM-neutrophil cluster among all cells and six BM-neutrophil subsets, and UMAP of unbiased clustering and cell annotation of BM-neutrophil subsets in groups WT and DM. (**C**) The proportion of BM-neutrophil subsets in groups WT and DM;*:p < 0.05. (**D**) Key marker genes of BM-neutrophil subsets. UMAP of key marker genes of BM-neutrophil subsets, along with the corresponding distribution of expression levels among 12 clusters and 6 BM-neutrophil subsets respectively. Key marker genes included Mpo, Slfn5, Retnlg, Orm1, Chit1 and Clec4d.

Proportional changes were as follows: BM-neutrophil_0 (50.19% → 39.72%), BM-neutrophil_1 (13.21% → 23.87%), BM-neutrophil_2 (15.47% → 11.01%), BM-neutrophil_3 (11.06% → 13.95%), BM-neutrophil_4 (5.75% → 5.64%), BM-neutrophil_5 (4.32% → 5.81%). Statistical significance was assessed with chi-square tests ($p < 0.05$ for all major changes) (Figure 2C).

Among the DEGs across the six neutrophil subsets, Arfgef1, Mrpl15, Ppplr42, Rblcc1, Rpl7, Sgk3, Tcea1, and Tram1 exhibited the most significant changes in expression levels. MPO, a heme protein crucial for neutrophil azurophilic granules,[26] was predominantly expressed in BM-neutrophil_0. Slfn5, a Schlafen family protein induced by interferon,[27] was mainly expressed in BM-neutrophil_1 and BM-neutrophil_0. Retnlg, also known as resistin-like gamma,[28] was expressed in BM-neutrophil_2 and BM-neutrophil_5. Orm1, an acute phase plasma protein,[29] was primarily found in BM-neutrophil_3 and BM-neutrophil_4. Chit1, a conserved chitinase secreted by activated macrophages,[30] was mainly expressed in BM-neutrophil_4. Clec4d, a receptor for trehalose-6,6'-dimycolate,[31] was expressed in both BM-neutrophil_2 and BM-neutrophil_5 (Figure 2D).

Differential directions and Monocle pseudotime trajectory expression pattern of 6 BM-neutrophil subsets were presented with a Heatmap presenting relative expressions of markers of BM-neutrophils along inferred trajectories in 6 BM-neutrophil subsets (Figure 3A and B).

Pseudotime analysis revealed two differentiation trajectories originating from BM-neutrophil_0. DEGs in trajectory 1 (Gm15818, Adhfe1, Arfgef1, Terf1, Rb1cc1, Mcmdc2, Sgk3) were associated with apoptosis regulation, hypoxia response, and cellular stress. Trajectory 2 DEGs (Tcf24, Rdh10, Lypla1, Cops5, Cspp1, Mybl1, Ncoa2, Snhg6, Vcpip1, Lactb2) suggest functional diversification. GO and KEGG enrichment showed upregulation in protein processing, oxidative phosphorylation, TNF signaling, osteoclast differentiation, IL-17 signaling, and lipid metabolism. Pathways labeled as "neurodegeneration" and "ALS" likely reflect shared stress and apoptosis mechanisms relevant to BM dysfunction in T2D (Figure 3C–H). Because BM-neutrophil_0 constituted the largest proportion of cells in group DM, we performed GO enrichment and KEGG pathway analyses on the upregulated DEGs identified in the BM-neutrophil_0 cluster, which indicated that the DEGs in BM-neutrophil_0 were primarily associated with the negative regulation of apoptotic processes, negative regulation of neuron apoptosis, and responses to hypoxia. The most common cellular components were the cytoplasm, extracellular region, and plasma membrane, while protein binding, identical protein binding, and hydrolase activity were the predominant molecular functions (Figure 3G). KEGG pathway analysis identified several highly enriched pathways among the DEGs, including neurodegeneration-related diseases, protein processing in the endoplasmic reticulum, amyotrophic lateral sclerosis, lipid and atherosclerosis, diabetic cardiomyopathy, NOD-like receptor signaling, oxidative phosphorylation, osteoclast differentiation, TNF signaling, Fc gamma R-mediated phagocytosis, and IL-17 signaling (Figure 3H). The top five upregulated DEGs were Vcan, Pla2g7, lghg2b, Gm43305, and Cfh, while the top five down-regulated DEGs were Prg2, Gata2, TRbc1, Cox6a2, and Lpl (Figure 3I and J).

Heterogeneity of B Cells

B cells were classified into precursor B cells (Pre_B, primarily expressing Ly6a, Cxcr5, and Ccr6) and naïve B cells (Naïve_B), primarily express IL2ra, Cd72, and Fam129c) (Figure 4A–D). Naïve_B increased from 64.29% to 82.03%, while Pre_B decreased from 35.71% to 17.97% (Figure 4C, $p < 0.01$). KEGG analysis revealed enrichment in antigen processing, insulin resistance, lipid metabolism, and NOD-like receptor signaling, reflecting functional alterations in immune regulation in T2D (Figure 4E and F). GO enrichment and KEGG pathway analyses were conducted for the upregulated DEGs in B cells, which revealed that the DEGs were predominantly associated with immune system processes, negative regulation of transcription by RNA polymerase II, and innate immune responses. The most common cellular components were the cytoplasm, nucleus, and cytosol, while the major molecular functions included protein binding, identical protein binding, and hydrolase activity (Figure 4E). KEGG pathway analysis identified several enriched pathways, including protein processing in the endoplasmic reticulum, lipid and atherosclerosis, antigen processing and presentation, estrogen signaling, NOD-like receptor signaling, measles, insulin resistance, and cholesterol metabolism (Figure 4F). The top five upregulated genes were Ddit4, Hist1h1b, Ighg2b, Ifi27l2a, and Cfh, while the top five downregulated genes were Ccl3, Klf4, Scd2, Hes1, and Lpl (Figure 4G and H).

https://doi.org/10.2147/JIR.S544316

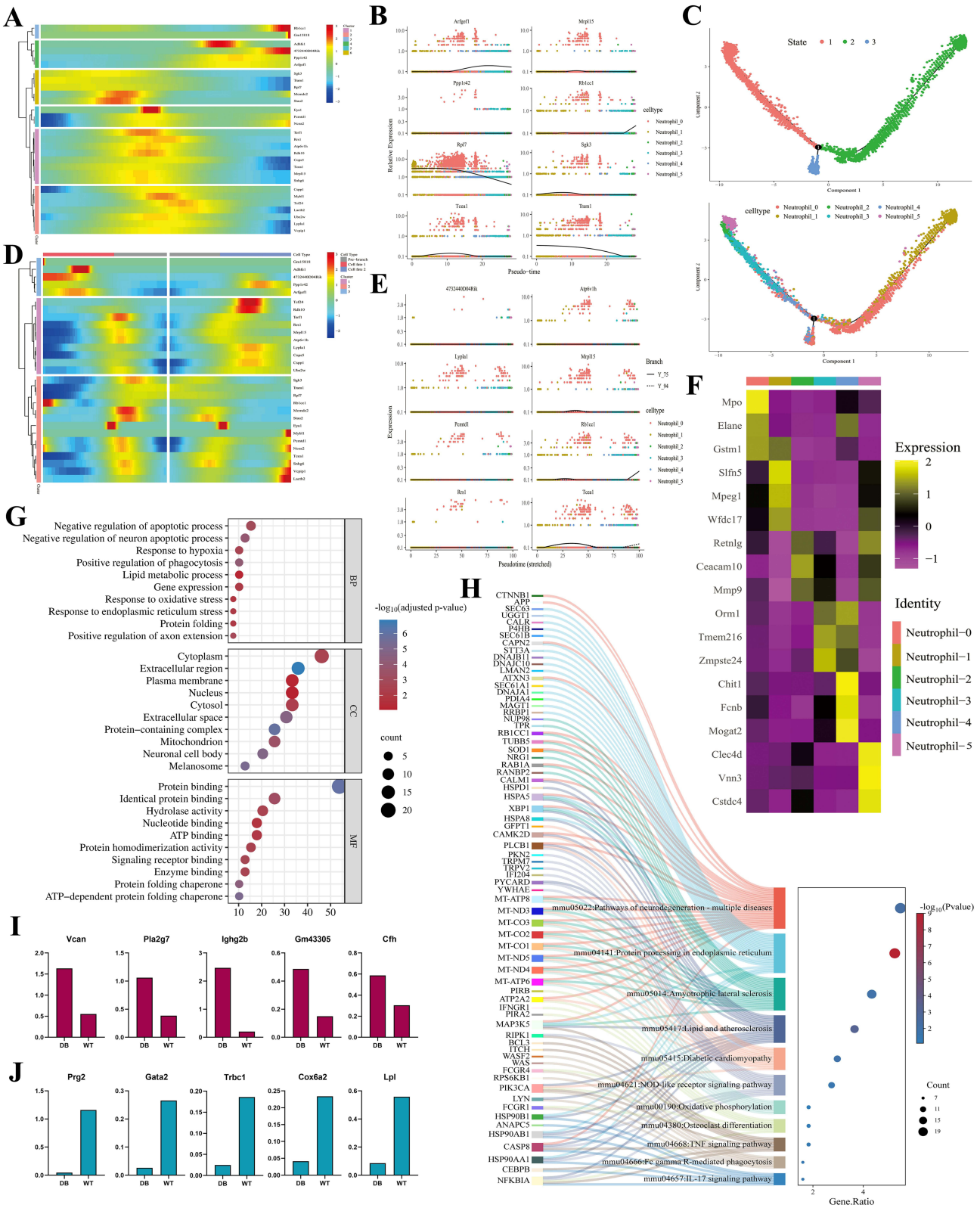

Figure 3 Differential trajectory of BM-neutrophil subsets and enrichment of DEGs. (**A-D**) Differential directions of 6 BM-neutrophil subsets: (**A**) Heatmap presenting relative expressions of markers of BM-neutrophils along inferred trajectories in 6 BM-neutrophil subsets. The red and blue branches correspond to the two differential directions. (**B**) Monocle pseudotime trajectory expression pattern of 6 BM-neutrophil subsets. (**C**) Pseudotime trajectories of the BM-neutrophil subsets. (**D**) The heatmap of branch point 1 shown in Figure 3C. (**E**) The top 8 key DEGs in these two cell fate. (**F**) Signature genes of BM-neutrophil subsets. Subset signature genes highlighted on left. Expression of signature genes (rows) across the cells (columns), the warmer the color, the higher the expression. (**G**) GO analysis of BM-neutrophil_1. Bubble diagram of upregulated DEGs of BM-neutrophil_1 enriched in GO analysis. (**H**) KEGG analysis of BMneutrophil_1. Bubble diagram of upregulated DEGs of BM-neutrophil_1 enriched in KEGG analysis. (**I-J**) The top 5 DEGs of BM-neutrophils. The top 5 upregulated DEGs between groups WT and DM (I). The top 5 downregulated DEGs between groups WT and DM (J).

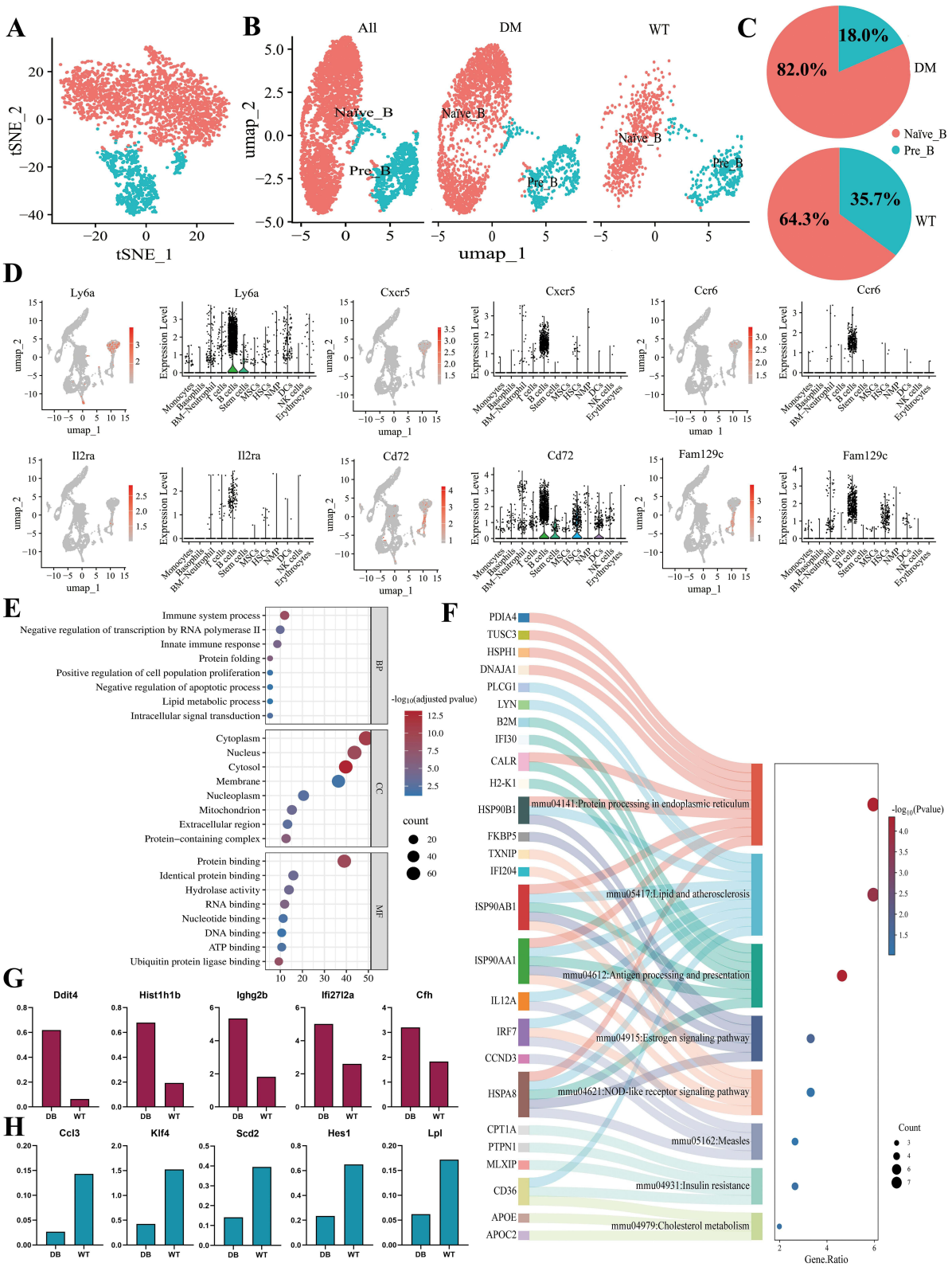

Figure 4 The characteristics of B cells between groups WT and DM. (**A**) The tSNE results of B cells cluster among all cells. (**B**) UMAP of the cluster of B cells among all cells, and UMAP of unbiased clustering and cell annotation of the subsets of B cells in groups WT and DM. (**C**) The proportion of the subsets of B cells in groups WT and DM. (**D**) Key marker genes of B cells subsets. UMAP of key marker genes of the subsets of B cells, along with the corresponding distribution of expression levels among 12 clusters. Key marker genes included Ly6a, Cxcr5, Il2ra, and Fam129c. (**E**) GO analysis of Naïve_B. Bubble diagram of upregulated DEGs of Naïve_B enriched in GO analysis. (**F**) KEGG analysis of Naïve_B. Bubble diagram of upregulated DEGs of Naïve_B enriched in KEGG analysis. (**G-H**) The top 5 DEGs of B cells. The top 5 upregulated DEGs between groups WT and DM (**G**). The top 5 downregulated DEGs between groups WT and DM (**H**).

https://doi.org/10.2147/JIR.S544316

Heterogeneity of Monocytes, T Cells, and DCs

Monocytes were subdivided into five subsets: monocyte_0 (primarily expressing Tprgl, S100a9, and S100a8), monocyte_1 (primarily expressing Ccnd1, Irf8, and Cst3), monocyte_2 (primarily expressing Apoc2, Mafb, and Ccr2), monocyte_3 (primarily expressing mt-Nd2, Mki67, and Zeb2), and monocyte_4 (primarily expressing Gpi1, Srgn, and Cd63) (Figure 5A–C). Monocytes (monocyte_0–4) showed shifts: monocyte_0 and monocyte_4 decreased, while monocyte_2 and monocyte_3 increased (Figure 5B). T cells were categorized into four subsets: γδ T cells (Tgd), primarily expressing Cd3e, Cd3d, and Thy1; natural killer cells (NK), primarily expressing Ncr1, Gzma, and Klra8; naïve T cells (T), primarily expressing Cd19, Plaur, and Cd74; and CD4+ T cells (CD4 T), primarily expressing Cd4, Foxp3, and Nrpl (Figure 5D–F). Proportional changes revealed that Tgd and naïve T cells decreased, and CD4+ T and NK cells increased (Figure 5E). DCs were classified into conventional DCs (cDC), primarily expressing Fcgr1, Ifi205, and Naaa; plasmacytoid DCs (pDC), primarily expressing Ccr9, Cox6a2, and Tlr7; and another DC subset, primarily expressing Clec9a, Sox4, and Calm. pDCs decreased while cDCs and the other subset slightly increased (Figure 5G–I).

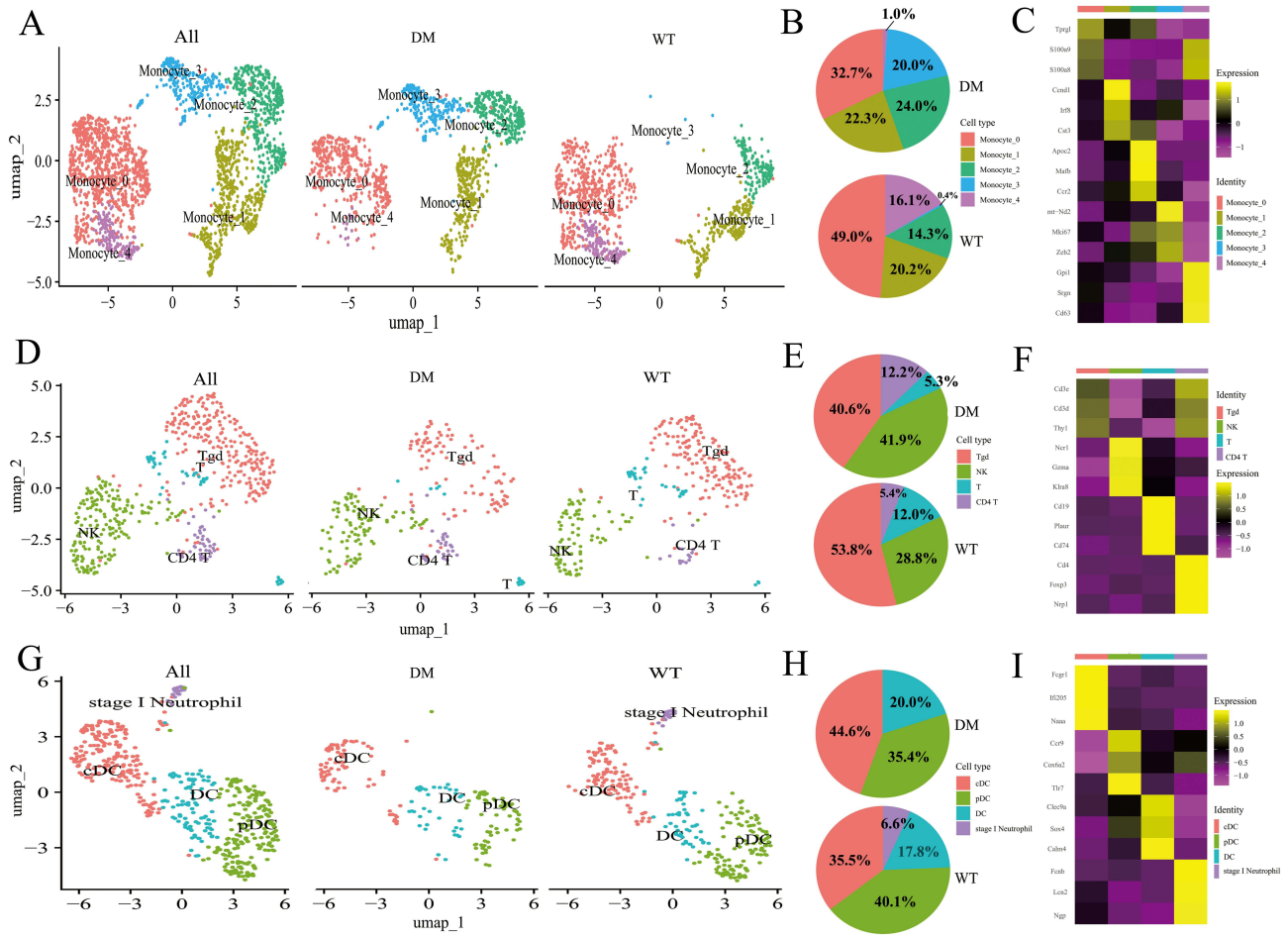

Figure 5 The characteristics of monocytes, T cells and DCs between groups WT and DM. (**A**) Five monocyte subsets: UMAP of unbiased clustering and cell annotation of the subsets of monocytes in groups WT and DM, and UMAP of unbiased clustering of the subsets of monocytes in groups WT and DM. (**B**) The proportion of the subsets of monocytes in groups WT and DM. (**C**) Signature genes of monocyte subsets. Subset signature genes highlighted on left. Expression of signature genes (rows) across the cells (columns), the warmer the color, the higher the expression. (**D**) Four T cells subsets: UMAP of unbiased clustering and cell annotation of the subsets of T lymphocytes in groups WT and DM, and UMAP of unbiased clustering of the subsets of T lymphocytes in groups WT and DM. (**E**) The proportion of the subsets of T cells in groups WT and DM. (**F**) Signature genes of T cells subsets. Subset signature genes highlighted on left. Expression of signature genes (rows) across the cells (columns), the warmer the color, the higher the expression. (**G**) Four dendritic cell subsets: UMAP of unbiased clustering and cell annotation of the subsets of DCs in groups WT and DM, and UMAP of unbiased clustering of the subsets of DCs in groups WT and DM. (**H**) The proportion of the subsets of DCs in groups WT and DM. (**I**) Signature genes of dendritic cell subsets. Subset signature genes highlighted on left. Expression of signature genes (rows) across the cells (columns), the warmer the color, the higher the expression.

Ratios of Immune Cells

We explored whether alterations in the ratios of immune cells within the bone marrow of WT and T2D mice. DM/WT ratios highlighted immune imbalances: monocytes/DCs ratio was highest, with BM-neutrophils/T cells and BM-neutrophils/DCs ratios increased, and BM-neutrophils/Naïve_B decreased (Figure 6A and B).

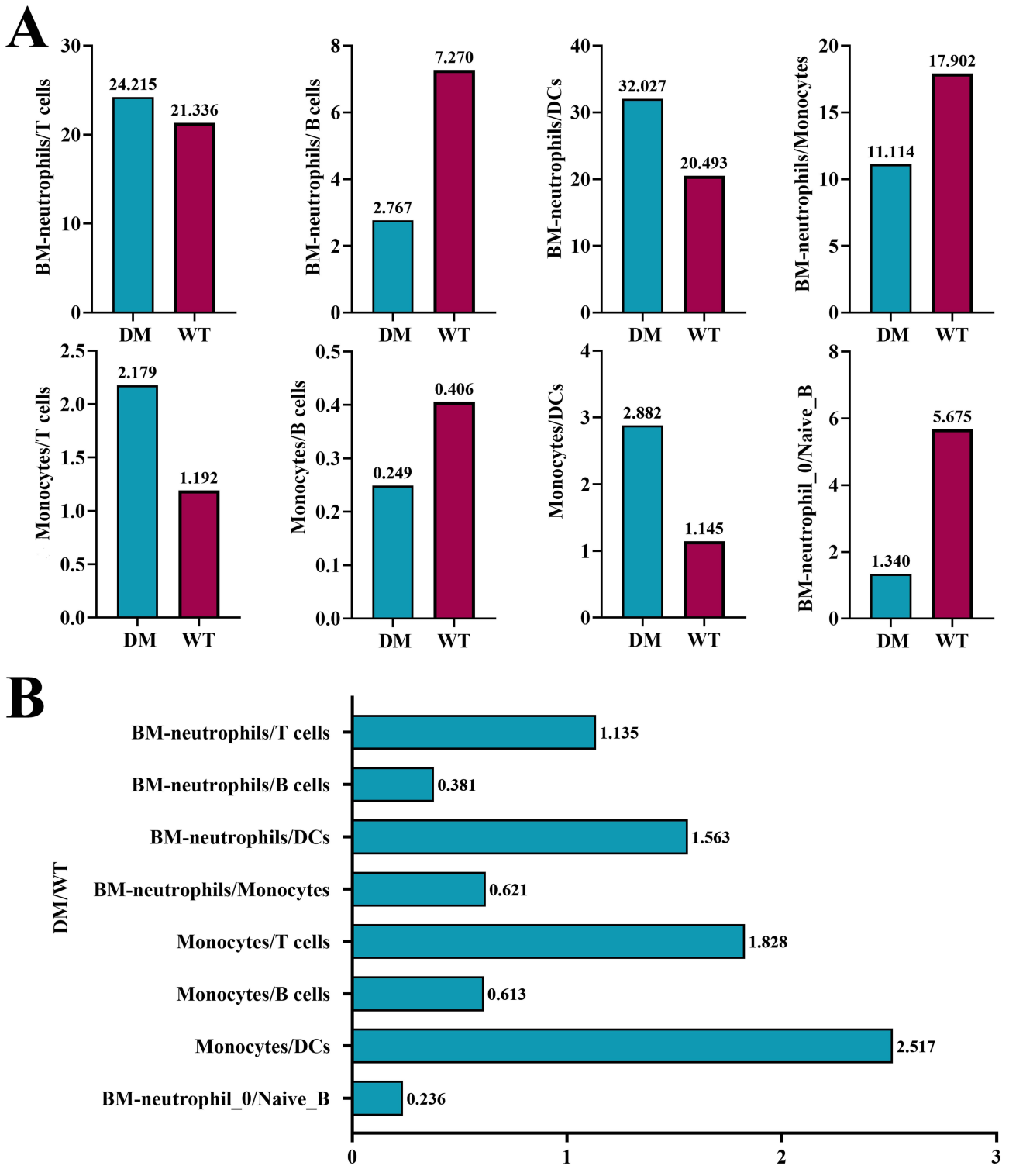

Figure 6 Identification of the ratio of immune cells between groups WT and DM. (**A**) The ratio of different immune cells. The ratio of BM-neutrophils/T cells, BM-neutrophils/B cells, BM-neutrophils/DCs, BM-neutrophils/monocytes, monocytes/T cells, monocytes/B cells, monocytes/DCs, BM-neutrophil_1/Naïve_B in groups WT and DM. (**B**) The rate of DB/WT among different immune cells. The RD/RC of BM-neutrophils/T cells, BM-neutrophils/B cells, BMneutrophils/DCs, BM-neutrophils/monocytes, monocytes/T cells, monocytes/B cells, monocytes/DCs, and BM-neutrophil_1/Naïve_B.

https://doi.org/10.2147/JIR.S544316

Cell-to-Cell Communication Analysis in the Bone Marrow of T2D Mice

To investigate the osteoimmune microenvironment in T2D mice, we conducted a cell-to-cell communication analysis using CellphoneDB. This analysis assessed interactions among various cell types in both WT and DM samples. Gaining insights into these cellular interactions will help clarify the underlying mechanisms of bone pathology and reveal potential targets for therapeutic intervention in T2D-associated bone loss. Figure 7A illustrates the differential number

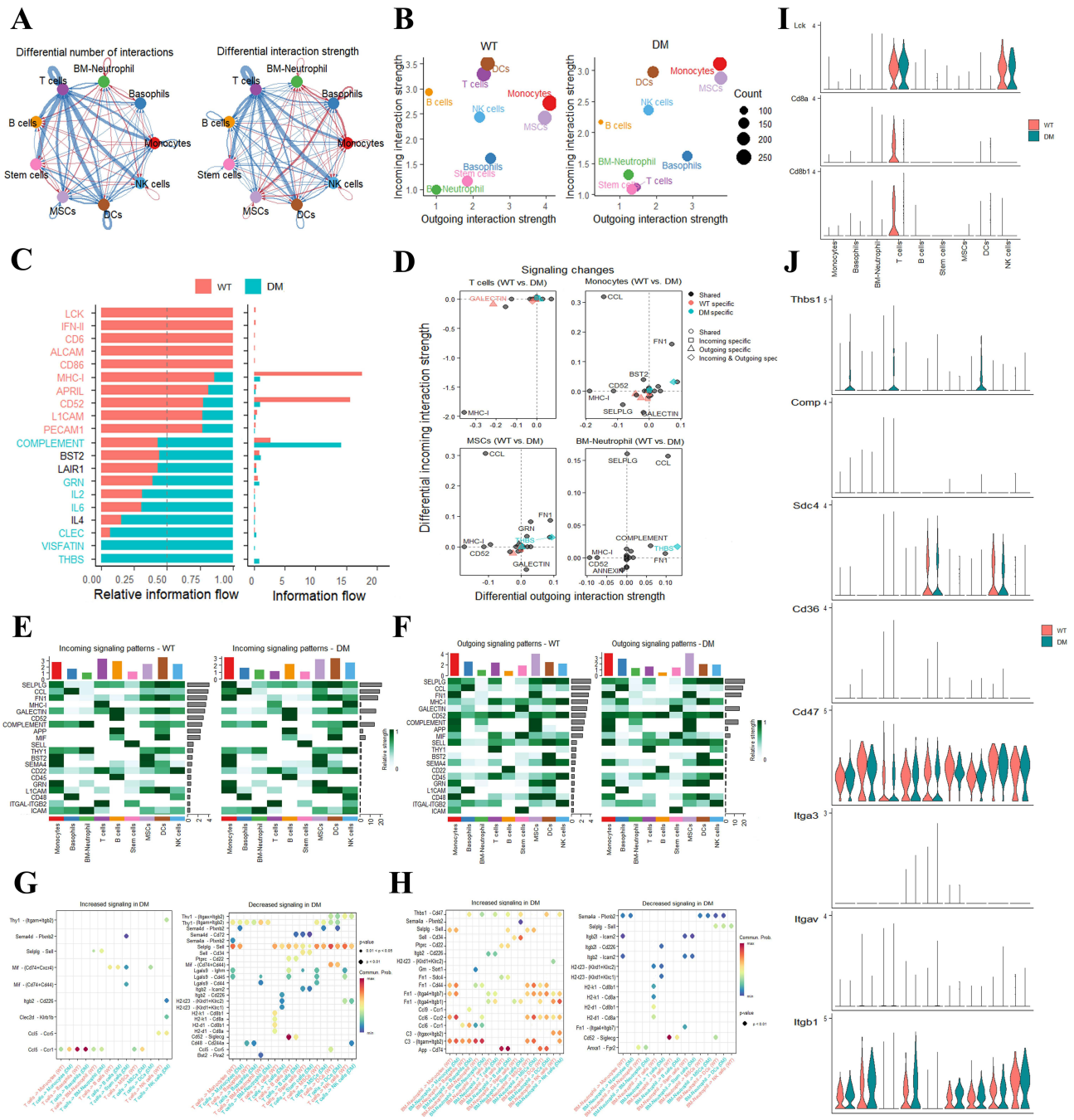

Figure 7 Cell-to-cell communication analysis using CellphoneDB to evaluate interactions between cell types in the WT and DM samples. (**A**) Differential number and strength of interactions between cell types in group DM and WT samples, with red indicating up-regulated and blue indicating down-regulated interactions. (**B**) Changes in cell roles: incoming and outgoing interaction strengths of immune cells. (**C**) Differences in signaling pathways of all cell types between WT and DM groups. (**D**) Differences in signaling pathways of T cells, monocytes, MSCs, and BM-Neutrophil between WT and DM groups. (**E-F**) Altered incoming (**E**) and outgoing (**F**) signaling patterns of immune cells in the WT and DM groups, respectively.(**G**) Changes ligand-receptor relationships between T cells and other immune cells in the DM group.((**H**) Changes in ligand-receptor relationships between BM-neutrophils and other immune cells in the DM group. (**I-J**) Relative expression of genes associated with the LCK and THBS signaling pathways cross all cell types in WT and DM groups.

and strength of interactions. CellphoneDB analysis revealed altered interaction strengths in T2D: incoming signals increased in BM-neutrophils, monocytes, MSCs, and decreased in B and T cells; outgoing signals increased in BM-neutrophils and basophils, decreased in T cells (Figure 7B and C indicates that differences in signaling pathways of all cell types between WT and DM groups.

Next, we examined differences in signaling pathways between WT and DM groups. Top enriched pathways in DM were THBS, VISFATIN, CLEC, IL4, IL6, whereas the top enriched pathways in the WT group were LCK, IFN-II, CD6, ALCAM, and CD86. Key ligand-receptor pairs included Thbs1–Cd47 (THBS pathway) and Clec4d–Fcgr2b (CLEC pathway), providing mechanistic insights into immune cell interactions in T2D (Figure 7D–H).

Specifically, Figure 7D indicates that CLEC was a specific outgoing signaling pathway for T cells in the DM group, while THBS was both an outgoing and incoming specific signaling pathway for monocytes, MSCs, and BM-neutrophils in the DM group. Figure 7E and F depicts the altered incoming and outgoing signaling patterns of immune cells in the WT and DM groups, respectively. To examine the ligand-receptor interactions among immune cells, we focused on the relationships between T cells and various other immune cell types. Our analysis revealed notable communication between T cells and Ccl5-Ccr1, confirming the molecular targets and bidirectional communication potential of T cells with other immune cells in the DM group (Figure 7G). Figure 7G also shows the changes in signaling involving ligand-receptor relationships between T cells and other immune cells in the DM group. Figure 7H illustrates the changes in signaling involving ligand-receptor relationships between BM-neutrophils and other immune cells in the DM group. Finally, Figures 7I and J present the relative expression of genes associated with the LCK and THBS signaling pathways in all cell types between the WT and DM groups.

Gene Expressions Validation by qRT-PCR Analysis

To validate gene expression patterns, quantitative real-time PCR (qRT-PCR) analysis was performed. The results demonstrated significantly reduced relative expression of FOSB, RELB, IL1B, MAP3K7, PPP3R1, TNF, TGFBR2, and SOCS3 in T2D bone marrow (Figure 8), consistent with scRNA-seq results, indicating strong concordance between the two methods.

Discussion

The advent of scRNA-seq has transformed our understanding of cellular heterogeneity and the complex molecular mechanisms underlying T2DM. By enabling the analysis of individual cells within heterogeneous tissues, scRNA-seq provides a high-resolution view of the cellular and molecular landscape, allowing us to dissect complex immune and stromal interactions within the bone marrow (BM). Our study leverages this technology to analyze BM cells from STZ-induced T2D mice, revealing significant alterations in immune cellular composition, subset functionality, and

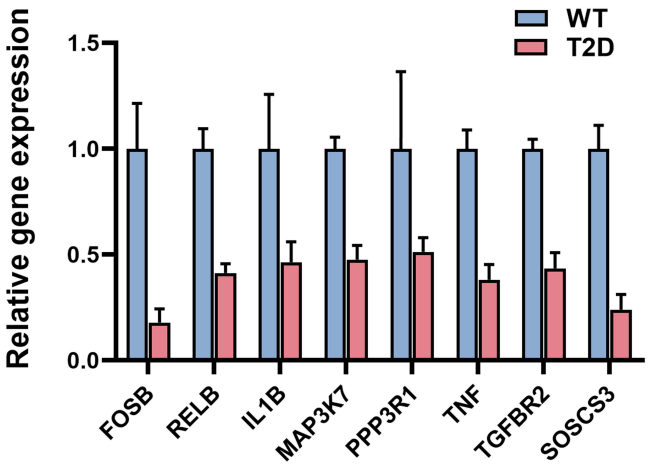

Figure 8 qRT-PCR Analysis of the expression levels of key genes in bone marrow of T2D mice and control samples.

https://doi.org/10.2147/JIR.S544316

intercellular communication. These findings offer valuable insights into how immune remodeling contributes to systemic inflammation, insulin resistance, and bone pathology in T2DM.

In total, twelve distinct cell clusters were identified within the BM, including monocytes, basophils, BM-neutrophils, T cells, B cells, stem cells, MSCs, HSCs, NMP, DCs, NK cells, and erythrocytes. When comparing T2D mice to wild-type controls, significant compositional changes were observed. Notably, T2D mice exhibited a substantial increase in B lymphocytes and MSCs, along with a decrease in BM-neutrophils and DCs, consistent with broad dysregulation of hematopoietic and immune cell populations in diabetes. These shifts may influence systemic inflammation, bone remodeling, and metabolic homeostasis, emphasizing the interconnected nature of immune dysfunction and bone pathology. Since immune cells in the BM are closely linked to both systemic inflammation and skeletal remodeling, these compositional changes may have profound implications for metabolic homeostasis and osteoimmune balance.[32–34]

Among the most striking findings was the pronounced decrease in BM-neutrophils, dropping from 66.56% in WT to 54.73% in T2D mice, which suggests altered neutrophil maturation or reprogramming. Neutrophils are central players in innate immunity, contributing to pathogen clearance, inflammation resolution, and bone remodeling via cross-talk with osteoclasts and osteoblasts. Their reduction in T2D may reflect impaired maturation or altered trafficking, consistent with prior studies linking neutrophil dysfunction to increased infection susceptibility and chronic inflammation in diabetes.[35–38] This dysfunction may also contribute to systemic insulin resistance. Dysregulated pathways such as CXCL12/CXCR3 could underlie aberrant neutrophil migration within BM, further impairing osteoimmune signaling. Although our computational analyses point to such mechanisms, functional assays—including NETosis, phagocytosis, or migration studies—will be essential to validate these predictions and clarify how neutrophil dysfunction contributes to bone pathology.

Conversely, B cells exhibited a notable increase in proportion, from 9.16% in WT to 19.78% in T2D mice, particularly within the Naïve_B subset. This expansion highlights adaptive immune activation in response to chronic metabolic stress. Activated B cells are known to produce pro-inflammatory cytokines and pathogenic antibodies, which can exacerbate insulin resistance and contribute to systemic inflammation. Previous studies revealed that B cells modulate immune responses and influence insulin resistance through antibody-mediated pathways and cytokine production, and their dysregulation has been associated with T2D complications, including cardiovascular disease and systemic inflammation.[39–42] The observed shift from Pre_B to mature B cell populations may reflect compensatory responses to T2D-induced chronic inflammation and metabolic stress that may exacerbate inflammatory signaling and systemic metabolic dysfunction.[43,44] These findings underscore the need to consider B cells as active contributors to T2D pathophysiology. Future studies could explore therapeutic targeting of B cell-derived cytokines, such as CCL4 and CCL5, to mitigate systemic inflammation.

Monocyte and T cell subsets exhibited significant alterations. Reductions in monocyte_0 and monocyte_4, coupled with increases in monocyte_2 and monocyte_3, suggest altered monocyte-mediated inflammation, likely contributing to chronic low-grade inflammation and insulin resistance. Prior studies have reported Cd36+ monocytes with diminished osteoclast potential in diabetic bone marrow, highlighting the importance of subset-level analyses for linking immune dysregulation to bone remodeling. Our data extend these findings, by providing subset-level resolution of T2D-specific monocyte alterations.[45–52] Similarly, T cell analysis revealed a decrease in γδ T cells and an increase in CD4+ T cells, particularly Th1 and Th17 subsets. While γδ T cells contribute to tissue homeostasis and immune surveillance, Th1/Th17 cells drive chronic inflammation and exacerbate metabolic dysregulation.[53–57] These results collectively suggest that T2D reshapes both innate and adaptive immune compartments, thereby directly influencing osteoimmune dynamics and bone remodeling capacity.

In addition, we observed a significant reduction in DCs, particularly plasmacytoid DCs (pDCs). Since pDCs are crucial for type I interferon responses and immune surveillance, their depletion could exacerbate chronic inflammation and impair host defense in T2D.[58–63] From an osteoimmunology perspective, DC–B cell crosstalk and DC-mediated regulation of osteoclastogenesis are key determinants of bone homeostasis. Their loss may therefore contribute to T2D-associated bone remodeling defects. Functional assays such as flow cytometry or in vitro osteoclastogenesis studies will be needed to confirm these transcriptomic observations.

Intercellular communication analysis using CellPhoneDB further highlighted T2D-specific signaling pathways, including THBS, CLEC, and IL-6. These interactions reinforce pro-inflammatory crosstalk between BM-neutrophils, monocytes, and MSCs, creating a feed-forward loop of immune activation. THBS signaling has known crosstalk with

TGF-β, which regulates osteoblast-osteoclast balance, linking immune dysregulation to altered bone metabolism in T2D. CLEC signaling was enriched in T cells, while THBS was prominent in monocytes, MSCs, and BM-neutrophils, supporting the notion of immune-mediated modulation of bone remodeling. Together, these cellular and molecular changes illustrate a network of immune dysregulation in the bone marrow that can drive systemic metabolic disturbances and bone remodeling defects in T2D.[64] KEGG pathway enrichment revealed terms such as "neurodegeneration" and "amyotrophic lateral sclerosis". While these may appear unrelated to BM, they likely reflect shared inflammatory mechanisms—including oxidative stress, mitochondrial dysfunction, and apoptosis—common to both neurodegenerative disorders and diabetic BM immune cells. We have prioritized pathways with established osteoimmunology relevance (RANKL/OPG, IL-17, TNF) while noting that neurodegeneration-associated enrichments indicate overlapping inflammatory processes. Our enrichment analyses of signaling pathways related to osteoclast differentiation and inflammation, such as TNF and IL-17 pathways, highlight the role of immune cell interactions in bone pathology and metabolic disorders.[65–67] Notably, Mac_OLR1 macrophages, known to support osteoclastogenesis, and Neut_RSAD2 neutrophils, which may impair osteoclast activity under diabetic stress, were transcriptionally linked to pathways such as AP-1 and FoxM1, bridging immune remodeling with T2D-specific skeletal phenotypes.[13,68] Previous osteoimmunology studies have shown that Mac_OLR1 macrophages promote osteoclast differentiation through RANKL and cytokine signaling, directly enhancing bone resorption.[69] Similarly, Neut_RSAD2 neutrophils can release reactive oxygen species and pro-inflammatory mediators that modulate osteoblast activity, potentially inhibiting bone formation.[69] These results strengthen the hypothesis that altered immune–bone signaling underlies diabetic skeletal pathology. However, functional perturbation studies—such as blocking antibodies or ligand–receptor inhibition—are needed to establish causal effects. Integration with spatial transcriptomics would also help clarify the anatomical context of these altered interactions.

Comparison with other diabetic contexts provides further perspective. In T1D models, neutrophil expansion and B cell reduction are often observed, whereas T2D mice displayed the opposite trend, suggesting divergent immunometabolic adaptations. This underscores the necessity of disease-specific studies to understand immune-bone crosstalk in diabetes.[19,70,71] This underscores the importance of disease-specific investigations of osteoimmune regulation. Importantly, the STZ-induced T2D model employed here reflects β-cell injury, which may not fully capture the complexity of human T2D. Incorporating db/db or diet-induced models, alongside human scRNA-seq datasets, would enhance translational relevance and help identify conserved versus model-specific immune alterations.

Relative to previous scRNA-seq studies[16,17] that broadly characterized myeloid and lymphoid compartments, our analysis provides deeper resolution of subset-specific changes and reveals novel ligand–receptor pathways underlying osteoimmune dysfunction in T2D. These findings advance our understanding of the BM microenvironment in diabetes and generate new hypotheses for targeted therapeutic intervention.

Although our results derive from an STZ-induced T2D mouse model, emerging human scRNA-seq data suggest parallels in immune dysregulation, including alterations in Naïve_B and monocyte subsets. Integrating human data, along with spatial transcriptomics, could map immune–stromal interactions with greater precision. Longitudinal studies across disease progression will be crucial for establishing causal relationships between immune remodeling and bone deterioration. These steps are essential for translating experimental observations into clinically meaningful therapies.

Several limitations warrant consideration. First, this study relied on a single publicly available dataset (GSE212726) with a small sample size (n=3/group), limiting statistical power and generalizability. Replication in larger and independent cohorts will be essential to confirm the reproducibility. Second, the STZ-induced diabetes model does not fully recapitulate the polygenic, obesity-associated, and insulin resistance–dominated pathophysiology of human T2DM, and STZ itself may exert off-target cytotoxic effects on bone marrow cells. Complementary models such as db/db or diet-induced T2D mice should be incorporated to enhance translational relevance. Third, this study relied solely on transcriptomic data without protein-level or functional validation. Gene expression changes may not directly reflect biological activity, and ligand–receptor interactions were inferred computationally rather than experimentally verified. Future validation through approaches such as flow cytometry, cytokine profiling, and in vitro functional assays will be essential. Similarly, ligand–receptor predictions were based on computational inference rather than experimental verification. Fourth, the analysis was restricted to a single time point (7 months), limiting insight into disease progression. Since immune remodeling in T2D is dynamic, longitudinal profiling would provide deeper understanding of temporal

immune and metabolic changes. Finally, the study did not integrate multi-omics approaches. Combining scRNA-seq with single-cell ATAC-seq, proteomics, or spatial transcriptomics could better capture transcriptional regulation, protein activity, and the spatial organization of immune–stromal interactions. Future work should integrate multiple datasets, complementary omics platforms, and longitudinal sampling to strengthen robustness.

Future studies could extend our findings by performing functional validation of key immune cell subsets and signaling pathways identified in T2D bone marrow. For example, in vivo or ex vivo experiments could assess the role of BM-neutrophil_0 and Naïve_B subsets in modulating systemic inflammation and insulin resistance. Targeted depletion or adoptive transfer experiments may clarify their causal contribution to metabolic dysfunction. Additionally, blocking or enhancing specific ligand-receptor interactions, such as THBS, CLEC, or IL-6 pathways, could reveal their functional impact on intercellular communication and bone remodeling. Longitudinal studies in T2D mouse models would also help determine how immune cell dynamics evolve over disease progression and influence bone health. Finally, integrating proteomic or metabolomic analyses could provide mechanistic insights into how altered signaling pathways contribute to chronic inflammation and metabolic dysregulation in T2D.

Conclusion

The present study, utilizing single-cell RNA sequencing (scRNA-seq), provides comprehensive insights into immune landscape alterations in the bone marrow of a T2DM mouse model. This approach has revealed significant changes in B cells, monocytes, T cells, and dendritic cells, along with altered intercellular signaling pathways, revealing nuanced T2D-specific reprogramming of the bone marrow immune microenvironment. These alterations are likely to influence osteoimmune interactions, affecting osteoclast and osteoblast activity, and thereby contributing to bone remodeling defects alongside systemic inflammation and insulin resistance. While these findings deepen our understanding of immune-mediated mechanisms in diabetic bone pathology, we acknowledge that mouse models may not fully replicate human T2DM pathology. Future studies should incorporate orthogonal datasets, human validation, longitudinal sampling, functional assays, and spatial transcriptomics to confirm these findings and enhance translational relevance.

Data Sharing Statement

The datasets presented in this study can be found in online repositories. The names of the repository/repositories and accession number(s) can be found below: https://www.ncbi.nlm.nih.gov/geo/, accession ID: GSE212726.

Ethics Approval and Consent to Participate

All protocols in this study were approved by the Committee on the Ethics of Animal Experiments of Shandong Provincial Hospital affiliated to Shandong First Medical University, in compliance with the Guide for the Care and Use of Laboratory Animals published by the NIH.

Author Contributions

All authors made a significant contribution to the work reported, whether that is in the conception, study design, execution, acquisition of data, analysis and interpretation, or in all these areas; took part in drafting, revising or critically reviewing the article; gave final approval of the version to be published; have agreed on the journal to which the article has been submitted; and agree to be accountable for all aspects of the work.

Funding

The design, collection, analysis, and interpretation of the data in the study were financially supported by the Jinan Clinical Medical Science and Technology Innovation Plan (NO. 202328065), the Natural Science Foundation of Shandong Province (No. ZR2021QH307; No. ZR2021MH013), and the Shandong Province Major Scientific and Technical Innovation Project (No. 2021SFGC0502). The authors, their immediate families, and any research foundations with which they are affiliated have not received any financial payments or other benefits from any commercial entity related to the subject of this article.

Disclosure

The authors declare that they have no competing interests.

References

1. Zheng Y, Ley SH, Hu FB. Global aetiology and epidemiology of type 2 diabetes mellitus and its complications. *Nat Rev Endocrinol*. 2018;14(2):88–98. doi:10.1038/nrendo.2017.151
2. Kahn SE, Cooper ME, Del Prato S. Pathophysiology and treatment of type 2 diabetes: perspectives on the past, present, and future. *Lancet*. 2014;383(9922):1068–1083. doi:10.1016/S0140-6736(13)62154-6
3. Morrison SJ, Scadden DT. The bone marrow niche for haematopoietic stem cells. *Nature*. 2014;505(7483):327–334. doi:10.1038/nature12984
4. Liu T, Zhang L, Joo D, et al. NF-kappaB signaling in inflammation. *Signal Transduct Target Ther*. 2017;2(17023). doi:10.1038/sigtrans.2017.23
5. Furman D, Campisi J, Verdin E, et al. Chronic inflammation in the etiology of disease across the life span. *Nature Med*. 2019;25(12):1822–1832. doi:10.1038/s41591-019-0675-0
6. Kanter JE, Hsu CC, Bornfeldt KE. Monocytes and macrophages as protagonists in vascular complications of diabetes. *Front. cardiovasc. med*. 2020;7(10). doi:10.3389/fcvm.2020.00010
7. Tripodo C, Sangaletti S, Piccaluga PP, et al. The bone marrow stroma in hematological neoplasms--a guilty bystander. *Nat Rev Clin Oncol*. 2011;8(8):456–466. doi:10.1038/nrclinonc.2011.31
8. Omatsu Y. Cellular niches for hematopoietic stem cells in bone marrow under normal and malignant conditions. *Inflamm regen*. 2023;43(1):15. doi:10.1186/s41232-023-00267-5
9. Wu PH, Joseph G, Saeed I, et al. Bone marrow adiposity alterations in type 2 diabetes are sex-specific and associated with serum lipid levels. *J Bone Miner Res*. 2023;38(12):1877–1884. doi:10.1002/jbmr.4931
10. Hofbauer LC, Busse B, Eastell R, et al. Bone fragility in diabetes: novel concepts and clinical implications. *Lancet Diabetes Endocrinol*. 2022;10(3):207–220. doi:10.1016/S2213-8587(21)00347-8
11. Shanbhogue M, Rosen DM, et al. Type 2 diabetes and the skeleton: new insights into sweet bones. *Lancet Diabetes Endocrinol*. 2016;4(2):159–173. doi:10.1016/S2213-8587(15)00283-1
12. Oikawa A, Siragusa M, Quaini F, et al. Diabetes mellitus induces bone marrow microangiopathy. *Arterioscler. Thromb. Vasc. Biol*. 2010;30(3):498–508. doi:10.1161/ATVBAHA.109.200154
13. Saito H, Gasser A, Bolamperti S, et al. TG-interacting factor 1 (Tgif1)-deficiency attenuates bone remodeling and blunts the anabolic response to parathyroid hormone. *Nat Commun*. 2019;10(1):1354. doi:10.1038/s41467-019-08778-x
14. Saltiel AR, Olefsky JM. Inflammatory mechanisms linking obesity and metabolic disease. *J Clin Invest*. 2017;127(1):1–4. doi:10.1172/JCI92035
15. Shaikh SR, Beck MA, Alwarawrah Y, et al. Emerging mechanisms of obesity-associated immune dysfunction. *Nat Rev Endocrinol*. 2024;20(3):136–148. doi:10.1038/s41574-023-00932-2
16. Hrovatin K, Fischer DS, Theis FJ. Toward modeling metabolic state from single-cell transcriptomics. *Mol Metabol*. 2022;57(101396). doi:10.1016/j.molmet.2021.101396
17. Jovic D, Liang X, Zeng H, et al. Single-cell RNA sequencing technologies and applications: a brief overview. *Clin trans med*. 2022;12(3):e694. doi:10.1002/ctm2.694
18. Song F, Lee WD, Marmo T, et al. Osteoblast-intrinsic defect in glucose metabolism impairs bone formation in type II diabetic male mice. *eLife*. 2023;12. doi:10.7554/eLife.85714
19. Zhong J, Mao X, Li H, et al. Single-cell RNA sequencing analysis reveals the relationship of bone marrow and osteopenia in STZ-induced type 1 diabetic mice. *J Adv Res*. 2022:41(145–158.doi: 10.1016/j.jare.2022.01.006.
20. Liu CC, McCaffrey EF, Greenwald NF, et al. Multiplexed Ion Beam Imaging: insights into Pathobiology. *Annu. Rev. Patholy*. 2022;17:403–423. doi:10.1146/annurev-pathmechdis-030321-091459
21. Efremova M, Vento-Tormo M, Teichmann SA, et al. CellPhoneDB: inferring cell-cell communication from combined expression of multi-subunit ligand-receptor complexes. *Nature Protocols*. 2020;15(4):1484–1506. doi:10.1038/s41596-020-0292-x
22. Zhang Q, Dong J, Zhang P, et al. Dynamics of transcription factors in three early phases of osteogenic, adipogenic, and chondrogenic differentiation determining the fate of bone marrow mesenchymal stem cells in rats. *Front Cell Develop Biol*. 2021;9(768316). doi:10.3389/fcell.2021.768316
23. Liu F, Dong J, Zhou D, et al. Identification of key candidate genes related to inflammatory osteolysis associated with vitamin e-blended uhmwpe debris of orthopedic implants by integrated bioinformatics analysis and experimental confirmation. *J Inflamm Res*. 2021;14:3537–3554. doi:10.2147/JIR.S320839
24. Liu F, Dong J, Zhang P, et al. Transcriptome sequencing reveals key genes in three early phases of osteogenic, adipogenic, and chondrogenic differentiation of bone marrow mesenchymal stem cells in rats. *Front Mol Biosci*. 2021;8(782054). doi:10.3389/fmolb.2021.782054
25. Liu N, Dong J, Li L, et al. Novel clinical insights into the pathogenesis of posttraumatic elbow stiffness: an expression profile analysis of contracted joint capsule in human. *J Inflamm Res*. 2025;18:167–182. doi:10.2147/JIR.S499986
26. Maiocchi SL, Ku J, Thai T, et al. Myeloperoxidase: a versatile mediator of endothelial dysfunction and therapeutic target during cardiovascular disease. *Pharmacol Ther*. 2021;221(107711). doi:10.1016/j.pharmthera.2020.107711
27. Kim ET, Dybas JM, Kulej K, et al. Comparative proteomics identifies Schlafen 5 (SLFN5) as a herpes simplex virus restriction factor that suppresses viral transcription. *Nature Microbiology*. 2021;6(2):234–245. doi:10.1038/s41564-020-00826-3
28. Uyar O, Dominguez JM, Bordeleau M, et al. Single-cell transcriptomics of the ventral posterolateral nucleus-enriched thalamic regions from HSV-1-infected mice reveal a novel microglia/microglia-like transcriptional response. *J Neuroinflammation*. 2022;19(1):81. doi:10.1186/s12974-022-02437-7
29. Rocanin-Arjo A, Cohen W, Carcaillon L, et al. A meta-analysis of genome-wide association studies identifies ORM1 as a novel gene controlling thrombin generation potential. *Blood*. 2014;123(5):777–785. doi:10.1182/blood-2013-10-529628
30. Belien J, Swinnen S, D'Hondt R, et al. CHIT1 at diagnosis predicts faster disability progression and reflects early microglial activation in multiple sclerosis. *Nat Commun*. 2024;15(1):5013. doi:10.1038/s41467-024-49312-y

31. Miyake Y, Toyonaga K, Mori D, et al. C-type lectin MCL is an FcRgamma-coupled receptor that mediates the adjuvanticity of mycobacterial cord factor. *Immunity*. 2013;38(5):1050–1062. doi:10.1016/j.immuni.2013.03.010
32. Liu N, Dong J, Li L, et al. Osteoimmune interactions and therapeutic potential of macrophage-derived small extracellular vesicles in bone-related diseases. *Int J Nanomed*. 2023;18:2163–2180. doi:10.2147/IJN.S403192
33. Zhang Q, Sun W, Li T, et al. Polarization behavior of bone macrophage as well as associated osteoimmunity in glucocorticoid-induced osteonecrosis of the femoral head. *J Inflamm Res*. 2023;16:879–894. doi:10.2147/JIR.S401968
34. Liu N, Dong J, Li L, et al. The FUNCTION and mechanism of anti-inflammatory factor metrnl prevents the progression of inflammatory-mediated pathological bone osteolytic diseases. *J Inflamm Res*. 2024;17:1607–1619. doi:10.2147/JIR.S455790
35. Guo G, Liu Z, Yu J, et al. Neutrophil function conversion driven by immune switchpoint regulator against diabetes-related biofilm infections. *Adv. Mater.* 2024;36(8):e2310320. doi:10.1002/adma.202310320
36. Umehara T, Mori R, Mace KA, et al. Identification of specific miRNAs in neutrophils of type 2 diabetic mice: overexpression of mirna-129-2-3p accelerates diabetic wound healing. *Diabetes*. 2019;68(3):617–630. doi:10.2337/db18-0313
37. Wong SL, Demers M, Martinod K, et al. Diabetes primes neutrophils to undergo NETosis, which impairs wound healing. *Nature Med*. 2015;21(7):815–819. doi:10.1038/nm.3887
38. Hughes MJ, McGettrick HM, Sapey E. Shared mechanisms of multimorbidity in COPD, atherosclerosis and type-2 diabetes: the neutrophil as a potential inflammatory target. *Eur. respir. rev.* 2020;29(155). doi:10.1183/16000617.0102-2019
39. Minton K. B1 B cells link gut dysbiosis and insulin resistance. *Nat Rev Immunol*. 2019;19(1):1. doi:10.1038/s41577-018-0096-1
40. DA W, Winer S, Shen L, et al. B cells promote insulin resistance through modulation of T cells and production of pathogenic IgG antibodies. *Nature Med*. 2011;17(5):610–617. doi:10.1038/nm.2353
41. Harmon DB, Srikakulapu P, Kaplan JL, et al. Protective role for b-1b b cells and igm in obesity-associated inflammation, glucose intolerance, and insulin resistance. *Arterioscler. Thromb. Vasc. Biol*. 2016;36(4):682–691. doi:10.1161/ATVBAHA.116.307166
42. Nishimura S, Manabe I, Takaki S, et al. Adipose natural regulatory b cells negatively control adipose tissue inflammation. *Cell Metab*. 2013;18(5):759–766. doi:10.1016/j.cmet.2013.09.017
43. Luck H, Khan S, Kim JH, et al. Gut-associated IgA(+) immune cells regulate obesity-related insulin resistance. *Nat Commun*. 2019;10(1):3650. doi:10.1038/s41467-019-11370-y
44. Ying W, Wollam J, Ofrecio JM, et al. Adipose tissue B2 cells promote insulin resistance through leukotriene LTB4/LTB4R1 signaling. *J Clin Invest*. 2017;127(3):1019–1030. doi:10.1172/JCI90350
45. Julla JB, Girard D, Diedisheim M, et al. Blood monocyte phenotype is a marker of cardiovascular risk in type 2 diabetes. *Circ. Res*. 2024;134(2):189–202. doi:10.1161/CIRCRESAHA.123.322757
46. Reddy MA, Amaram V, Das S, et al. lncRNA DRAIR is downregulated in diabetic monocytes and modulates the inflammatory phenotype via epigenetic mechanisms. *JCI Insight*. 2021;6(11). doi:10.1172/jci.insight.143289
47. Junqueira C, Crespo A, Ranjbar S, et al. FcgammaR-mediated SARS-CoV-2 infection of monocytes activates inflammation. *Nature*. 2022;606(7914):576–584. doi:10.1038/s41586-022-04702-4
48. Westcott DJ, Delproposto JB, Geletka LM, et al. MGL1 promotes adipose tissue inflammation and insulin resistance by regulating 7/4hi monocytes in obesity. *J Exp Med*. 2009;206(13):3143–3156. doi:10.1084/jem.20091333
49. Wang H, Guo Z, Xu Y. Association of monocyte-lymphocyte ratio and proliferative diabetic retinopathy in the U.S. population with type 2 diabetes. *J Transl Med*. 2022;20(1):219. doi:10.1186/s12967-022-03425-4
50. Kitade H, Sawamoto K, Nagashimada M, et al. CCR5 plays a critical role in obesity-induced adipose tissue inflammation and insulin resistance by regulating both macrophage recruitment and M1/M2 status. *Diabetes*. 2012;61(7):1680–1690. doi:10.2337/db11-1506
51. Merad M, Martin JC. Pathological inflammation in patients with COVID-19: a key role for monocytes and macrophages. *Nat Rev Immunol*. 2020;20(6):355–362. doi:10.1038/s41577-020-0331-4
52. Petit V, Parcelier A, Mathe C, et al. TRIM33 deficiency in monocytes and macrophages impairs resolution of colonic inflammation. *EBioMedicine*. 2019;44:60–70. doi:10.1016/j.ebiom.2019.05.037
53. Li P, Li K, Yuan W, et al. 1alpha,25(OH)(2)D(3) ameliorates insulin resistance by alleviating gammadelta T cell inflammation via enhancing fructose-1,6-bisphosphatase 1 expression. *Theranostics*. 2023;13(15):5290–5304. doi:10.7150/thno.84645
54. Tao L, Liu H, Gong Y. Role and mechanism of the Th17/Treg cell balance in the development and progression of insulin resistance. *Mol Cell Biochem*. 2019;459(1–2):183–188. doi:10.1007/s11010-019-03561-4
55. Bertola A, Ciucci T, Rousseau D, et al. Identification of adipose tissue dendritic cells correlated with obesity-associated insulin-resistance and inducing Th17 responses in mice and patients. *Diabetes*. 2012;61(9):2238–2247. doi:10.2337/db11-1274
56. Savage TM, Fortson KT, de Los Santos-Alexis K, et al. Amphiregulin from regulatory T cells promotes liver fibrosis and insulin resistance in non-alcoholic steatohepatitis. *Immunity*. 2024;57(2):303–318e306. doi:10.1016/j.immuni.2024.01.009
57. Li Y, Lu Y, Lin SH, et al. Insulin signaling establishes a developmental trajectory of adipose regulatory T cells. *Nat Immunol*. 2021;22(9):1175–1185. doi:10.1038/s41590-021-01010-3
58. Moller SH, Wang L, Ho PC. Metabolic programming in dendritic cells tailors immune responses and homeostasis. *Cell. Mol. Immunol*. 2022;19(3):370–383. doi:10.1038/s41423-021-00753-1
59. Ye Y, Gaugler B, Mohty M, et al. Plasmacytoid dendritic cell biology and its role in immune-mediated diseases. *Clin. Transl. Immunol*. 2020;9(5):e1139. doi:10.1002/cti2.1139
60. Macdougall CE, Wood EG, Solomou A, et al. Constitutive activation of beta-catenin in conventional dendritic cells increases the insulin reserve to ameliorate the development of type 2 diabetes in mice. *Diabetes*. 2019;68(7):1473–1484. doi:10.2337/db18-1243
61. Hernandez-Garcia E, Cueto FJ, Cook ECL, et al. Conventional type 1 dendritic cells protect against age-related adipose tissue dysfunction and obesity. *Cell. Mol. Immunol*. 2022;19(2):260–275. doi:10.1038/s41423-021-00812-7
62. Kelly B, O'Neill LA. Metabolic reprogramming in macrophages and dendritic cells in innate immunity. *Cell Res*. 2015;25(7):771–784. doi:10.1038/cr.2015.68
63. Hanc P, Gonzalez RJ, Mazo IB, et al. Multimodal control of dendritic cell functions by nociceptors. *Science*. 2023;379(6639):eabm5658. doi:10.1126/science.abm5658

64. Thimmappa PY, Vasishta S, Ganesh K, et al. Neutrophil (dys)function due to altered immuno-metabolic axis in type 2 diabetes: implications in combating infections. *Human Cell*. 2023;36(4):1265–1282. doi:10.1007/s13577-023-00905-7
65. Yoshitaka T, Ishida S, Mukai T, et al. Etanercept administration to neonatal SH3BP2 knock-in cherubism mice prevents TNF-alpha-induced inflammation and bone loss. *J Bone Miner Res*. 2014;29(5):1170–1182. doi:10.1002/jbmr.2125
66. Li J, Ayoub A, Xiu Y, et al. TGFbeta-induced degradation of TRAF3 in mesenchymal progenitor cells causes age-related osteoporosis. *Nat Commun*. 2019;10(1):2795. doi:10.1038/s41467-019-10677-0
67. Li JY, D'Amelio P, Robinson J, et al. IL-17A Is increased in humans with primary hyperparathyroidism and mediates pth-induced bone loss in mice. *Cell Metab*. 2015;22(5):799–810. doi:10.1016/j.cmet.2015.09.012
68. Yang Y, Ren D, Peng B, et al. Promotion of inflammatory response in mice with diabetes periodontitis: regulation of forkhead box protein M1 silencing to mediate activator protein-1 via reactive oxygen species production. *CytoJournal*. 2024;21(72). doi:10.25259/Cytojournal_143_2024
69. Yang W, Wang Y, Mo K, et al. Single-cell RNA sequencing reveals multiple immune cell subpopulations promote the formation of abnormal bone microenvironment in osteoporosis. *Sci Rep*. 2024;14(1):29493. doi:10.1038/s41598-024-80993-z
70. Sundararaghavan V, Mazur MM, Evans B, et al. Diabetes and bone health: latest evidence and clinical implications. *Ther. Adv. Musculoskelet. Dis*. 2017;9(3):67–74. doi:10.1177/1759720X16687480
71. Huang J, Xiao Y, Zheng P, et al. Distinct neutrophil counts and functions in newly diagnosed type 1 diabetes, latent autoimmune diabetes in adults, and type 2 diabetes. *Diabetes/Metab Res Rev*. 2019;35(1):e3064. doi:10.1002/dmrr.3064